

Tuning the Size and Shape of Zeolite L-Based Inorganic–Organic Host–Guest Composites for Optical Antenna Systems**

By Silke Megelski and Gion Calzaferri*

Fine tuning of the size of zeolite L crystals in a large range is possible by changing the composition of the starting gel for otherwise constant reaction conditions. We describe a convenient way to prepare different crystalline materials in the size range of 30 nm up to 3000 nm. Representative data on the morphology, the pore volume, the size distribution and the optical antenna system behavior for light harvesting and transport are reported. We have extended the investigations on energy migration in pyronine-loaded zeolite L crystals as donor molecules, modified with oxonine as luminescent acceptors (traps) at the crystal ends. The preparation procedure reported and the extended zeolite materials now available lead to a large improvement of the energy migration efficiency.

1. Introduction

Zeolite L is a crystalline aluminosilicate where connected SiO_4 and AlO_4 tetrahedra give rise to one-dimensional channels arranged in a hexagonal structure.^[1–3] It was found to be a very suitable host material to develop new organic–inorganic composites with optical antenna properties for light harvesting and transport.^[4–9] Other hosts that were studied for obtaining new optical materials are AIPO-5 and zeolite ZSM-5.^[10–14] Control of the shape and the size of the crystals is a necessary prerequisite for particular applications. Large crystals of a few hundred to a few thousand nm are very useful for studying the optical and photophysical properties of host–guest dye–zeolite composites on single crystals by means of optical microscopy methods.^[9,15] Crystals in the range of a few tenths to a few hundred nanometers are needed for high-efficiency optical antenna materials, useful as fluorescent microprobes, or for developing a new generation of dye-sensitized solid state solar cells or light-emitting diodes.^[16] We therefore focus in this article on zeolite L crystals of varying size and shape.

Zeolite L can be synthesized under hydrothermal conditions without an organic template in a wide range of gel compositions.^[1] The size and the morphology depend on the composition of the starting gel, the nature of the starting material and therefore also on its history, but also on the reaction conditions and temperature. A number of observations concerning zeolite L synthesis have been published.^[17–20] It is often difficult to

reproduce the reported results because the information given is not sufficiently detailed. We have therefore investigated the influence of the static/dynamic crystallization conditions and of the composition and nature of the starting materials on the synthesis product, and we describe a convenient way to prepare different zeolite L materials in the size range of 30 nm up to 3000 nm. Representative data on important material properties such as the morphology, the pore volume, the size distribution, and the optical antenna system behavior are reported.

2. General

2.1. Zeolite L

In the classical sense, zeolites are crystalline aluminosilicates with a large variety of well-defined three-dimensional frameworks. $[\text{SiO}_4]^{4-}$ and $[\text{AlO}_4]^{5-}$ tetrahedra are the primary building units. They form different secondary building units, depending on their spatial arrangement. The structure of zeolite L is illustrated in Figure 1. It consists of cancrinite cages (ϵ -cage) linked by double 6-rings (D6R). These units form columns in the c -direction, which are connected by oxygen bridges and thus give rise to 12-membered rings with a free diameter of 7.1 Å.^[2] As a consequence, zeolite L consists of one dimensional channels, running through the whole crystal, with a largest free diameter of about 12.6 Å and a unit cell length of 7.5 Å.^[21] The main channels are linked via non-planar 8-rings, which form an additional two dimensional channel system with about 1.5 Å ring openings.^[22] The hexagonal structure of zeolite L material is visible in the scanning electron microscopy (SEM) picture shown in Figure 1c. It also illustrates that the shape of the crystals can be described reasonably well by assuming cylinder morphology. The number of channels lying parallel to the c -axis is equal to $0.265(d_z)^2$, where d_z is the diameter of the cylinder in nanometers. Hence, a crystal with a 600 nm diameter consists of about 96 000 parallel channels, as an example.

[*] Prof. G. Calzaferri, Dr. S. Megelski
Department of Chemistry and Biochemistry
University of Berne
Freiestrasse 3, CH-3012 Berne (Switzerland)
E-mail: gion.calzaferri@iac.unibe.ch

[**] We thank R. Bühler for his contribution to the zeolite L synthesis, A. Schindler for adsorption measurements, Dr. I. Florian and Dr. H. Reichert from POROTEC for helpful discussions on adsorption measurements, and H. Peters from ALV for the DLS measurements and evaluation. This work was supported by the Swiss National Science Foundation Project NFP 47(4047-057481) and NF 2000-061259.

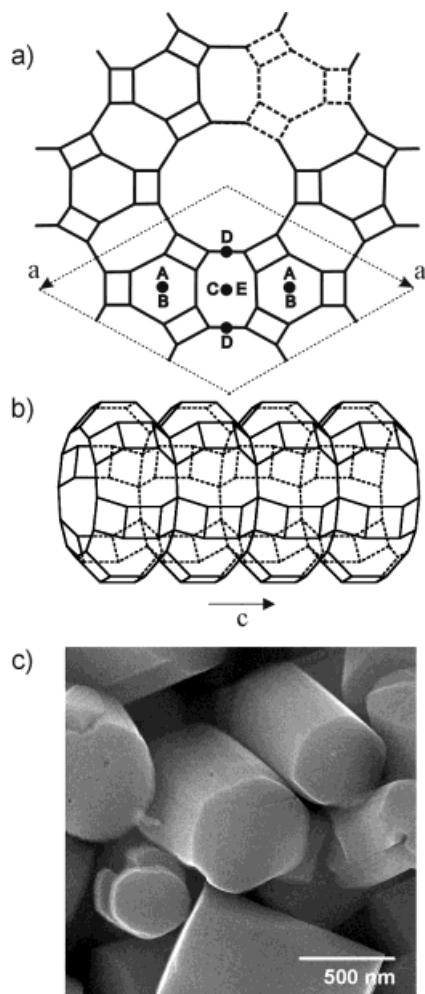


Fig. 1. a) Zeolite L framework with the different cation positions A to E and the ϵ -cage (dashed) viewed perpendicularly to the c -axis. b) Side view of the 12-ring channel along the c -axis. c) SEM picture of zeolite L.

Zeolite L has an anionic framework, because of the trivalent aluminum. Its stoichiometry with monovalent cations M^+ is $(M)_{9-\delta}[Al_{9-\delta}Si_{27+\delta}O_{72}] \cdot nH_2O$, where δ depends on the synthesis procedure and n corresponds to the crystal water. Four different sites (A, B, C, D), where the charge compensating cations in fully hydrated ($n \approx 21$) zeolite L can be located, have been reported.^[22] A is in the center of the D6R-unit, B is in the center of the ϵ -cage, C lies midway between the centers of two adjacent ϵ -cavities, and D is inside the main channel near the wall of the 8-ring. Dehydrated zeolite L shows an additional cation site located midway between two adjacent sites A and is indicated as E, see Figure 1a. More recently Sato et al. confirmed the cation sites B, D, and E, but not A and C by X-ray Rietveld analysis.^[23] The ion-exchange properties of zeolite L have been investigated in several studies.^[24–27] From this we know that cations in different sites have different mobilities. Only those on site D seem to be exchangeable at room temperature in aqueous environment. The water molecules in the large cavities of zeolite L were reported to behave like an intra-crystalline liquid, whereas they seem to build clusters around the cations in the smaller pores.^[1] In very thin layers

water can be removed to a large extent under vacuum conditions even at room temperature,^[28] while in bulk material a higher temperature is needed.^[29] Data on water desorption measurements of different zeolite L materials have recently been reported.^[30] The inner pore volume can be determined from adsorption measurements with, e.g., H_2O , N_2 , Ar, O_2 , Kr.^[1] The specific surface area and the free pore volume of zeolite L are best determined by means of Ar adsorption at 87 K. Experiments should be carried out at small relative pressure and in small steps with sufficiently long waiting periods to make sure that equilibrium conditions are maintained. The smaller the pore size of the material, the smaller the relative pressure for adsorption in micropores. Ar adsorption isotherms reveal detailed information about variations in pore size, e.g., as a consequence of different cations^[31] or between different zeolites.^[32] Microporous materials show type I adsorption isotherms (IUPAC classification),^[33] which are characterized by a steep increase in the small relative pressure region followed by an almost horizontal plateau before reaching the saturation pressure of the adsorbates. The specific surface area can be deduced by means of the Langmuir model. Nevertheless, the Brunauer–Emmett–Teller (BET) method, a further evolution of the Langmuir model, has become the standard method for surface area determination of powders and porous materials in the last 50 years, and it is also often used for microporous materials. Actually, BET cannot be used for surface area determination if the solid contains pores of molecular dimensions, which is the case for zeolite L.^[34–36] But for comparative studies of different zeolite L samples it is sufficient to evaluate the BET surface area in the region of p/p_0 where the BET plot is linear. If the isotherm almost goes parallel to the relative pressure scale up to $p/p_0 \approx 1$, the pore volume (Gurvich volume) can be determined from the amount of Ar adsorbed at this point.^[37] Furthermore, the micropore distribution of a zeolite with cylindrically shaped pores can be evaluated by applying the method of Saito/Foley.^[38]

2.2. Control of Crystallinity, Morphology, and Size of Zeolite L Crystals

We are interested in a set of procedures for fine-tuning the size of disc-like or cylindrical zeolite L crystals in the range of a few tenths to a few thousand nm. The material should be of high crystallinity and narrow size distribution. Zeolite synthesis is known to be complex because gel composition, alkalinity, temperature, time, and nature of the starting materials do contribute in a specific way to the success of crystallization.^[39] The growth mechanism of zeolite L is not well understood despite of the fact that the first report on its successful preparation dates from 1962. Breck and Acara described the synthesis of zeolite L containing K^+ , as well as K^+ and Na^+ as exchangeable cations, starting from an aluminate and silicate solution.^[40] They also reported several cations for ion-exchange reactions. The progress in zeolite L synthesis until 1994 was reviewed by Ernst and Weitkamp, who also specifically illustrated the synthesis of cylinder-shaped zeolite L crystals.^[19] Some patents

appeared in the 1990s in which procedures to prepare zeolite L crystallites with hexagonal cross-section in the order of some micrometers are disclosed.^[17,18,41,42] The preparation of “ultra-fine zeolite L” crystals in the range of 30 to 60 nm, which seem to have the tendency to form nanoclusters, was published more recently.^[43–45] Meng and coworkers investigated the influence of the reaction temperature, the reaction time, and the composition of the reaction mixture (specifically the SiO₂/Al₂O₃, the H₂O/Al₂O₃, and the K₂O/Al₂O₃ ratio) on the resulting product.^[44] They found that an optimal range of the K₂O/Al₂O₃ ratio to obtain pure zeolite L is 10–12.5, if SiO₂/Al₂O₃: 20; H₂O/Al₂O₃: 400. Lovallo and Tsapatsis propose a gel-to-zeolite transformation through local rearrangements of the former and explain in this way the formation and the structure of the zeolite L nanoclusters.^[20] They conclude that the morphology of the precursor gel plays a dominant role in determining the zeolite shape and size. More recently, Ko and Ahn reported the synthesis and characterization of zeolite L in the size regime of 0.3 μm to 1.4 μm by varying the reaction of a mixed K⁺/Na⁺ system.^[46] Therefore, we know that zeolite L crystallites generally become larger when increasing the SiO₂/Al₂O₃ or the H₂O/Al₂O₃ ratio within a given range of component composition. On the other hand, an increase in the amount of K₂O (i.e., also higher alkalinity) in the starting gel results in smaller zeolite L crystals. The pretreatment of the raw material, i.e., the preparation of a separate aluminate and silicate solution in aqueous KOH and aging them at elevated temperature before combining, as well as a shorter reaction time, yields small crystallites. Increase of the synthesis temperature leads to shorter reaction times and an increased crystallinity of the product. It follows that it is necessary to control the synthesis parameter very carefully in order to obtain reproducible results. We add that materials with zeolite L structure in the size regime of some micrometers have been obtained by partially replacing Al³⁺ with Fe³⁺.^[47]

2.3. Organic Guests

Organic dye molecules tend to form aggregates, which are known to cause fast thermal relaxation of the electronically excited states. They are usually unstable under irradiation for many conditions, but especially when present as monomers. Protection against bimolecular reactions but also unwanted isomerization reactions is possible by encapsulating them in an appropriate host such as a zeolite. Dye–zeolite composites sometimes represent a supramolecular organization with new material properties.^[10,48,49] Zeolite L was found to be a versatile host into which a large variety of cationic and neutral dyes and combinations of them can be incorporated.^[8,30,50–52] We have especially been interested in designing efficient optical antenna functionalities for light harvesting, transport, and capturing as illustrated in Figure 2.

The two cationic dyes pyronine (Py⁺), as a donor and oxonine (Ox⁺), as an acceptor were found to be very versatile for advancing this research. They can be incorporated into zeo-

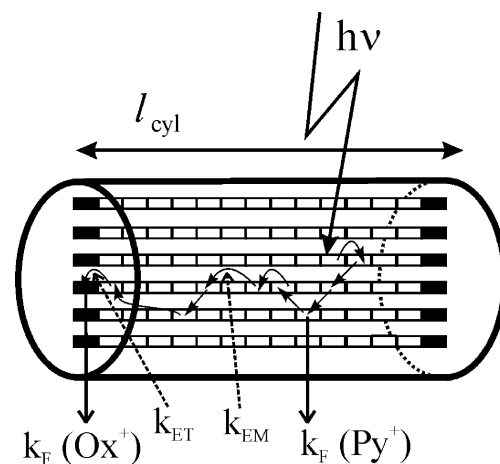
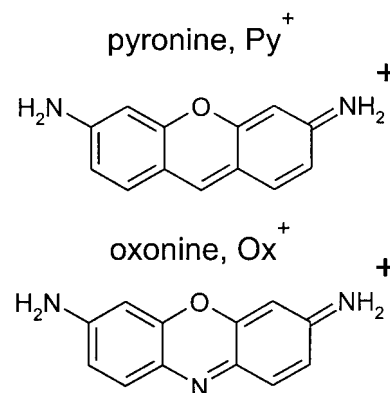


Fig. 2. Representation of a bi-directional antenna. A crystal of length l_{cyl} with channels occupied by donor molecules, Py⁺ (shaded rectangles), and with acceptors, Ox⁺ (black rectangles), at their ends, which act as luminescent traps. The arrows indicate the direction of energy migration. Once the excitation energy has reached an Ox⁺ there is no way back. k_{F} indicates the rate constant of fluorescence for the corresponding dyes, k_{ET} is the rate constant for energy transfer from Py⁺ to Ox⁺ and k_{EM} for energy migration among the Py⁺ molecules.



lite L by means of ion exchange, where they are present as monomers because of the restricted space. In this form they have a high fluorescence quantum yield and favorable spectral properties; see Figure 3.^[7,8] Insertion of the dyes can be visualized in different ways by means of a fluorescence microscope^[6,9] and the optical anisotropy of Ox⁺ loaded zeolite L has recently been investigated in detail.^[15] The dye molecules are located at sites along the linear channels of zeolite L. For Ox⁺ and Py⁺, the largest atom-to-atom distance of which is about 11.3 Å, the length of a site is two unit cells. The occupation probability p of the sites with a dye is equal to the number of occupied sites divided by the number of sites available. Using this notion the Förster type energy transfer^[53] and the energy migration rate k_{ij} from a molecule i to a molecule j in this material can be expressed by:^[5]

$$k_{ij} = \frac{9(\ln 10)}{128\pi^5 N_A n^4} \cdot \frac{\Phi_i}{\tau_i} \cdot G_{ij} J_{ij} p_i p_j \quad (1)$$

where Φ_i and τ_i [s⁻¹] are the fluorescence quantum yield and the intrinsic fluorescence lifetime of the donor, N_A is the Avogadro number, n is the refractive index of the medium, G_{ij} [Å⁻⁶]

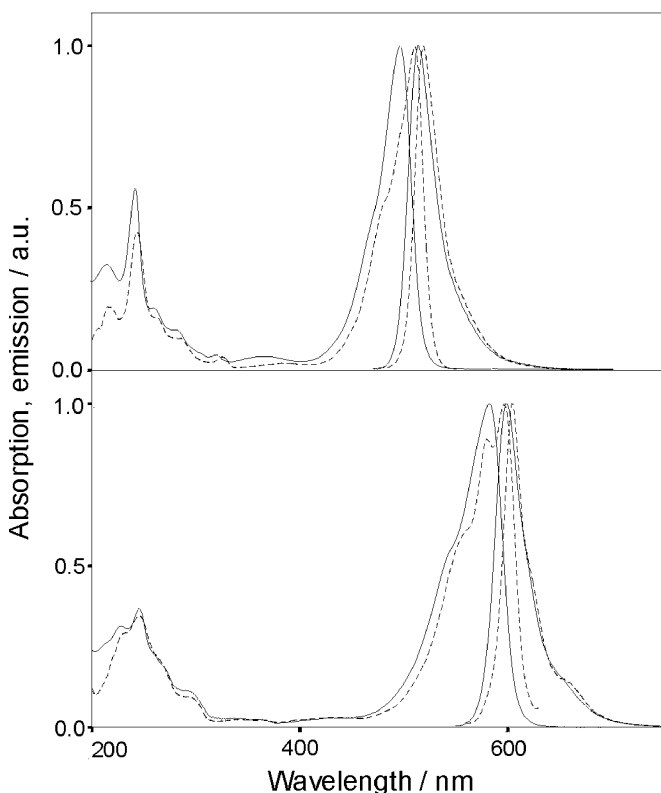


Fig. 3. Upper: Py^+ absorption and fluorescence (λ_{ex} : 460 nm) spectra in aqueous solution (solid) and excitation (λ_{em} : 560 nm) and fluorescence (λ_{ex} : 460 nm) spectra in zeolite L suspension (dashed). Lower: Ox^+ absorption and fluorescence (λ_{ex} : 560 nm) spectra in aqueous solution (solid) and excitation (λ_{em} : 640 nm) and fluorescence (λ_{ex} : 560 nm) spectra in zeolite L suspension (dashed).

represents the geometrical constraints of the sites in the crystal and the relative ordering of the transition moments, p_i and p_j are the occupation probabilities of the sites with excited donors i and acceptors j in the ground state, and J_{ij} [$\text{cm}^3 \text{M}^{-1}$] is the spectral overlap integral between the donor emission and the acceptor absorption spectrum.

The channels of zeolite L are loaded with Py^+ and their ends are modified with Ox^+ , in the antenna illustrated in Figure 2. Ox^+ acts as a luminescent trap, which gets excited via radiationless energy transfer from an excited Py^+ molecule. If radiationless relaxation is not considered, Ox^+ can lose its excitation energy only by fluorescence, as it cannot transfer the energy back to Py^+ because of its lower excitation energy. Fluorescence of excited Py^+ , internal conversion and intersystem crossing compete with the energy migration and energy transfer processes. The arrangement shown in Figure 2 allows us to investigate the efficiency of energy migration among the Py^+ molecules along the crystal as a function of its lengths and also of its loading, by measuring the front-back trapping efficiency $T_{\text{FB},\infty}$. The front-back trapping efficiency is equal to the ratio of luminescence intensity emitted by the acceptor Ox^+ (I_{ox}) divided by the total fluorescence intensity ($I_{\text{ox}} + I_{\text{py}}$).^[5,7]

$$T_{\text{FB},\infty} = \frac{I_{\text{ox}}}{I_{\text{py}} + I_{\text{ox}}} \quad (2)$$

3. Results

We report results on different zeolite L synthesis procedures, on Ar adsorption and dynamic light scattering (DLS) measurements of selected materials, and on energy migration in Py^+ loaded crystals modified with Ox^+ as acceptors as a function of the Py^+ loading and, specifically, as a function of the crystal size. The formal composition of the synthesis gel is expressed in the following as ($a \text{K}_2\text{O} - b \text{Al}_2\text{O}_3 - c \text{SiO}_2 - d \text{H}_2\text{O}$). In the zeolite literature this is often expressed as a ratio with respect to the SiO_2 content ($\text{SiO}_2/\text{Al}_2\text{O}_3$: α ; $\text{H}_2\text{O}/\text{SiO}_2$: β ; $\text{K}_2\text{O}/\text{SiO}_2$: γ). We prefer to use the former kind of writing because it is better understood by chemists who actually intend to reproduce a specific procedure, although the information content is the same in both cases.

3.1. Synthesis

Fine tuning of the size of zeolite L crystals in the range of 30 nm to 3000 nm is possible by changing the composition (a, b, c, d) of the starting gel for otherwise constant reaction conditions.

3.1.1. Influence of the Water Content

We started with the gel composition ($2.99 \text{K}_2\text{O} - 1 \text{Al}_2\text{O}_3 - 10.70 \text{SiO}_2 - 169.3 \text{H}_2\text{O}$) and increased the amount of water in seven steps up to 332.4. In each case a good quality zeolite L was obtained. The size of the resulting crystals increased with increasing water content of the reaction mixture. We illustrate this by means of the electron microscopy (EM) pictures in Figure 4. The amount of water can only be varied to some extent independently of the other components because zeolite L is not formed outside of a certain composition range. The water content of a synthesis gel with the formal composition ($2.55 \text{K}_2\text{O} - 1 \text{Al}_2\text{O}_3 - 9.72 \text{SiO}_2 - 161.3 \text{H}_2\text{O}$) can not exceed 201.5, because otherwise no zeolite L is formed. However, a small amount of the largest zeolite L crystals we have made is formed in the $201.5 \text{H}_2\text{O}$ gel (3000 nm length and a diameter of 1200 nm). The well-shaped crystals show a very nice cylindrical morphology with hexagonal cross section and a smooth surface. They can easily be separated from residual products by sedimentation.

3.1.2. Influence of the $\text{K}_2\text{O}/\text{SiO}_2$ Ratio

The influence of the amount of potassium hydroxide present in the gel was studied by starting with the formal composition ($2.55 \text{K}_2\text{O} - 1 \text{Al}_2\text{O}_3 - 9.74 \text{SiO}_2 - 161.3 \text{H}_2\text{O}$). The K_2O content was increased in five steps up to 3.29. Increasing the alkalinity results in shorter crystals with an almost constant diameter but an increasing intergrowth at the crystal ends. The smallest zeolite L crystals result from the gel of the highest alkalinity. They are disc shaped with a length of about 300 nm and a diameter

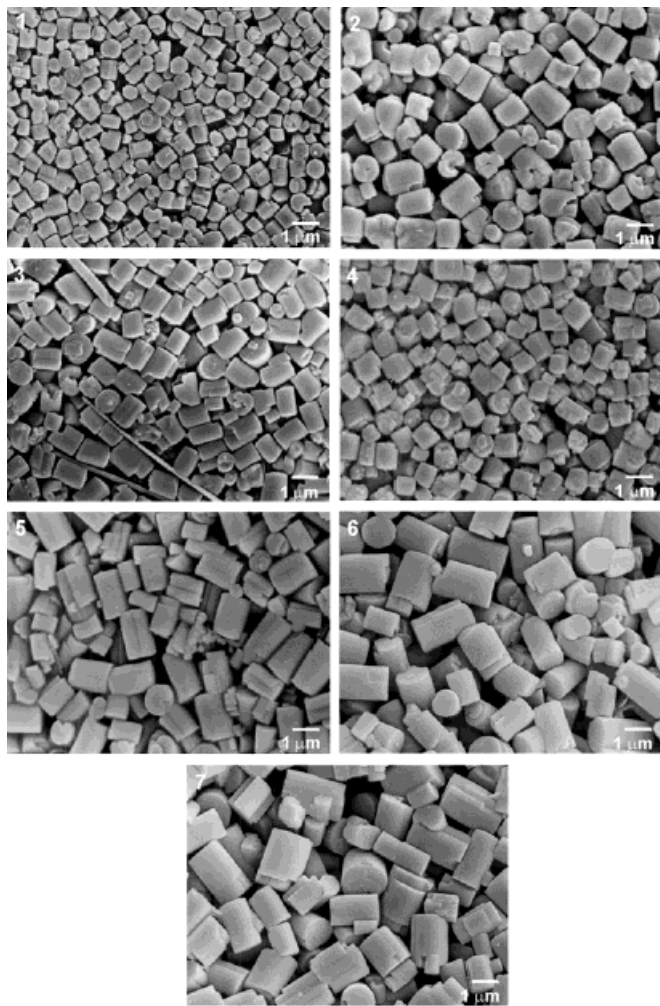


Fig. 4. EM pictures of zeolite L from the starting gel composition ($2.99\text{K}_2\text{O}-1\text{Al}_2\text{O}_3-10.7\text{SiO}_2-d\text{H}_2\text{O}$) and increasing amount of H_2O , $d =$: 1, 169.3; 2, 182.0; 3, 194.6; 4, 199.2; 5, 250.7; 6, 299.7; 7, 332.4.

of about 650 nm. We conclude that the relative growth in c -direction decreases with increasing alkalinity of the gel. This is accompanied by an increase of the Al^{3+} content of the zeolite L crystals. The results are illustrated in Figure 5 and Table 1.

3.1.3. Influence of the Substitution of K^+ by Na^+

The influence of the partial substitution of K^+ by Na^+ is illustrated for the following composition ($2.99\text{K}_2\text{O}-1\text{Al}_2\text{O}_3-10.70\text{SiO}_2-169.0\text{H}_2\text{O}$). Up to 50% of the K^+ can be substituted by Na^+ in this gel. 50% Na^+ in the synthesis gel yields zeolite L as a by-product. When more Na^+ was added, no zeolite L was obtained. In general, addition of Na^+ results in increasingly larger and better quality crystals with decreasing intergrowths, as can be seen in Figure 6.

3.1.4. Zeolite L Nanocrystals

Based on the above results and on previous reports^[44,45] the outcome of a very high alkalinity with the composition

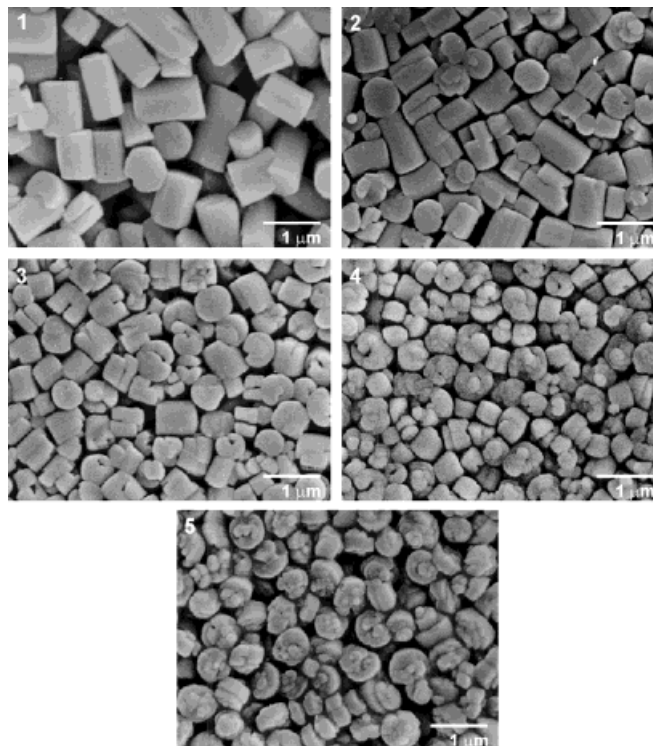


Fig. 5. EM pictures of zeolite L from a starting gel composition ($a\text{K}_2\text{O}-1\text{Al}_2\text{O}_3-9.74\text{SiO}_2-161\text{H}_2\text{O}$) and increasing amount of K_2O , $a =$: 1, 2.55; 2, 2.70; 3, 2.84; 4, 3.14; 5, 3.29.

Table 1. $\text{K}_2\text{O}/\text{SiO}_2$ ratio of the synthesis gel and resulting $\text{SiO}_2/\text{Al}_2\text{O}_3$ ratio of the zeolite L crystals as determined by EDX analysis.

| $\text{K}_2\text{O}/\text{SiO}_2$ (synthesis gel) | $\text{SiO}_2/\text{Al}_2\text{O}_3$ (crystal) |
|--|---|
| 0.262 | 6.8 |
| 0.277 | 6.5 |
| 0.292 | 6.5 |
| 0.323 | 6.4 |
| 0.339 | 6.0 |

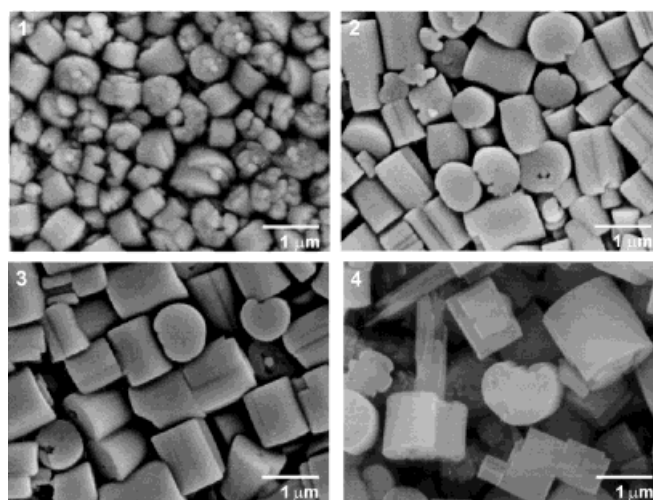


Fig. 6. EM pictures of zeolite L after substitution of K^+ by Na^+ in a starting gel with the molar composition ($2.99\text{K}_2\text{O}-1\text{Al}_2\text{O}_3-10.7\text{SiO}_2-168-170\text{H}_2\text{O}$). The amount of Na^+ is 1) 20 mol-%, 2) 34 mol-%, 3) 47 mol-%, 4) 50 mol-%.

(10 K₂O–1 Al₂O₃–20 SiO₂–400 H₂O) was tested for the preparation of very small crystals. We obtained a product that can be described as zeolite nanocrystals with a size of about 30 nm. They tend to agglomerate into larger clusters of 100 nm diameter, as illustrated in the transmission electron microscopy (TEM) image in Figure 7a. The transmission X-ray diffraction (XRD) pattern of this material in comparison with that of zeolite L microcrystals is shown in Figure 7b, which also shows the expected line-broadening due to the small size.

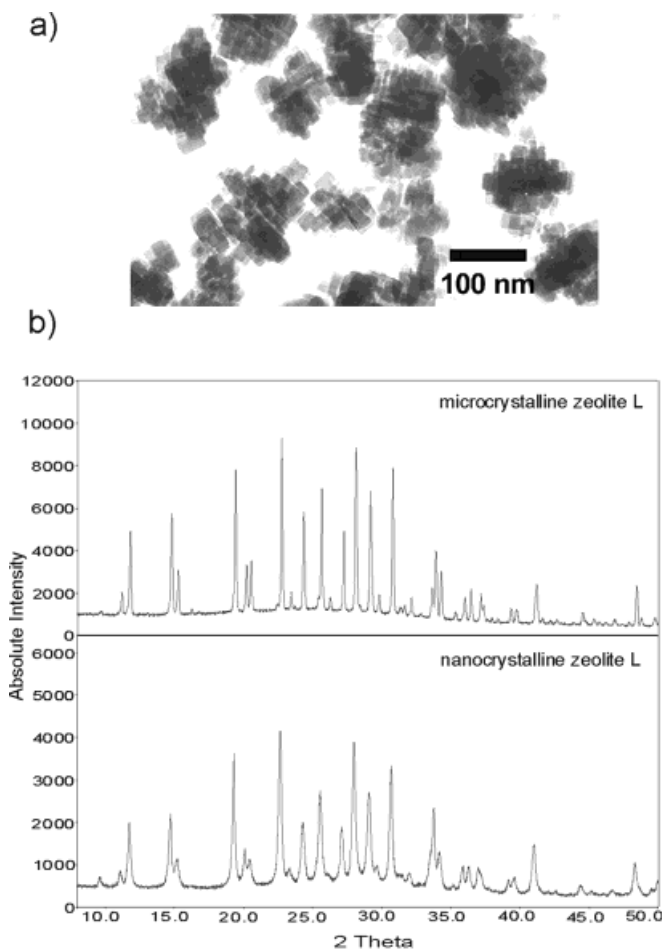


Fig. 7. a) TEM image of zeolite L nanocrystals that form nanoclusters. b) X-ray powder diffraction pattern (taken in transmission mode) in the 2θ -range 8–50° for zeolite L microcrystals (upper) and zeolite L nanocluster (lower). The (100) peak at $2\theta = 5.54$ was omitted for better comparison of the peaks at higher 2θ values.

3.1.5. Comparison of Crystal Growth under Static and Dynamic Conditions

We found that the crystallization time at 433 K can be reduced by a factor of 3 when using dynamic conditions during the crystal growth. The materials obtained for the same composition were observed to consist of somewhat larger crystals with smoother surfaces.

3.2. Characterization

3.2.1. Dynamic Light Scattering

The size distribution of some materials was tested by means of DLS in addition to the EM measurements. We report the observation made on the material shown in picture 5 of Figure 5, as an example. The mass-weighted distribution function of the dynamic light scattering experiment results in Figure 8, showing a mono modal very narrow size distribution from which a hydrodynamic radius of 295 nm was calculated.

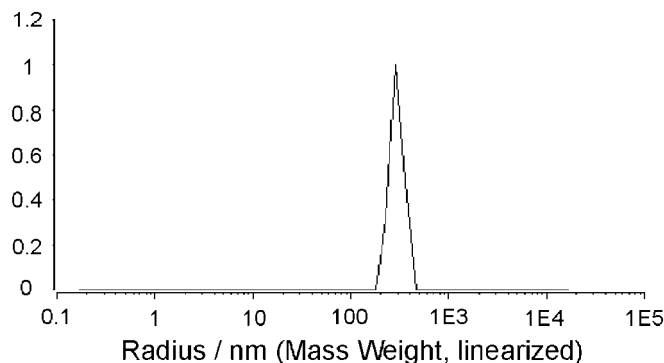


Fig. 8. Mass weighted particle size distribution of the zeolite L sample shown in picture 5 of Figure 5 from DLS measurements measured by ALV.

3.2.2. Ar Adsorption

Such measurements are a suitable tool to test zeolites with respect to their pore structure.^[31,32] All zeolite L samples show microporous behavior, which results in a type I adsorption isotherm. We illustrate in Figure 9 adsorption isotherms of the same material as above (picture 5, Fig. 5) and of a commer-

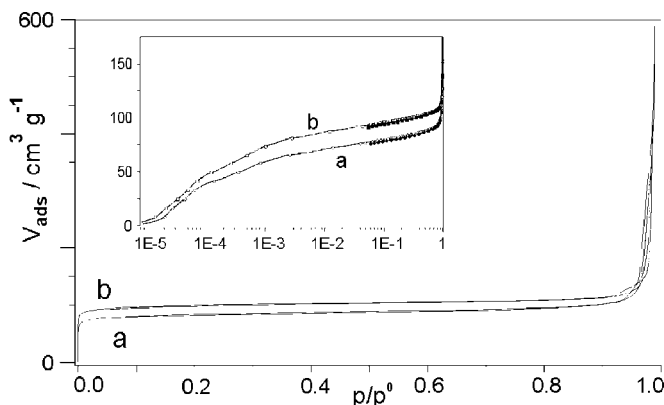


Fig. 9. Argon adsorption isotherms. a) Of zeolite L from Union Carbide measured at 87 K, b) of the same zeolite as in Figure 8. The insert shows a semi-logarithmic plot of the adsorption isotherm.

cially available zeolite L (Union Carbide). The isotherms show that the commercial (a) and the self-synthesized zeolite L (b) have different adsorption capacities. The higher increase in the first region of the adsorption isotherm of self-synthesized zeolite L reveals that a larger amount of Ar is adsorbed by the

micropores of this sample. Afterwards both isotherms run parallel to the relative pressure scale, which reflects the small outer surface area. The self-synthesized zeolite L samples show a higher specific surface area and a larger pore volume, independent of the model used for the calculations; Table 2. The difference in the adsorption capacity between the two samples can be clearly seen in the micropore filling at small relative pressure in the logarithmic representation of the isotherm, shown as insert in Figure 9.

Table 2. Specific surface areas and specific pore volumes of commercial and self-synthesized zeolite L (picture 5, Fig. 5). V_t : determined from Ar adsorption isotherm at $p/p^0 = 0.95$. V_{mp} : Cumulative pore volume determined with the method of Saito/Foley.

| zeolite L | S_{Langmuir} [m ² g ⁻¹] | S_{BET} [m ² g ⁻¹] | V_t [mL g ⁻¹] | V_{mp} [mL g ⁻¹] |
|-------------------------------|--|---|--------------------------------|-----------------------------------|
| commercial (Union Carbide) | 333.3 | 257.5 | 0.149 | 0.11 |
| synthesized | 393.7 | 307.8 | 0.158 | 0.13 |

3.3. Energy Migration

We have extended the investigations on energy migration in Py⁺ loaded zeolite L crystals, modified with Ox⁺ as luminescent acceptor (trap) at the crystal ends. The improved preparation procedure reported in the experimental section and the extended zeolite materials now available lead to a large improvement of the front-back trapping efficiency, Equation 2, with respect to the earlier reports.^[7,8] The two important parameters we can vary in order to test the energy migration efficiency are the loading with donor molecules Py⁺, which we express as p_{py} , and the length l_{cyl} of the cylindrical crystals. The loading with acceptors Ox⁺ corresponded to 1 to 2 molecules at both ends of each channel, on average. Since experiments were carried out on thin layers on a quartz substrate and not on single crystals, the p_{py} , l_{cyl} , and p_{ox} are average values. The front-back trapping efficiency can be tested by exciting the crystals at a wavelength where the acceptor absorption is negligible.

3.3.1. Trapping Efficiency as a Function of the Donor Concentration p_{py}

We expect from Equation 1 an increasing energy migration rate and therefore an increasing front-back trapping efficiency with increasing p_{py} . This was quantitatively investigated for zeolite L crystals with a length of approximately 650 nm. We prepared a wide range of Py⁺ loading ranging from 0.007 to 0.182, modified with Ox⁺ as luminescent acceptors, and we report data of six experiments in Figure 10 and Table 3a, recorded upon excitation at 470 nm. The spectra are scaled to the same height at the Py⁺ emission maximum, which allows better comparison. The Ox⁺ emission has its maximum at 605 nm and its intensity increases strongly with increasing p_{py} from sample 1 to 6. In fact, the trapping efficiency increases from 0.36 up to 0.74. This means that more and more of the

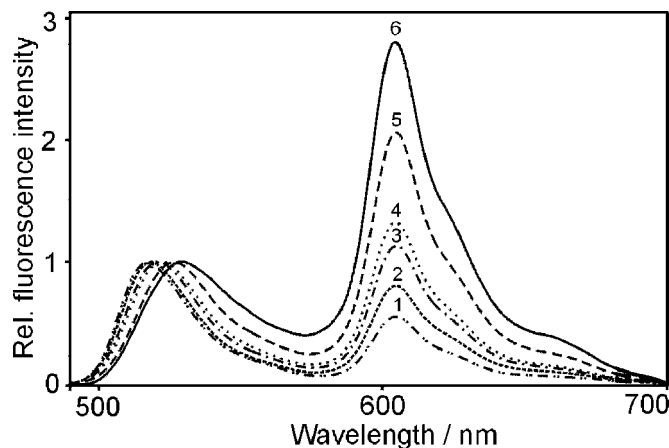


Fig. 10. Fluorescence intensity after specific excitation of only Py⁺ at 470 nm (scaled to the same height at the maximum of the Py⁺ emission) of Py⁺ loaded and Ox⁺ modified zeolite L crystals (650 nm length/600 nm diameter) as a function of Py⁺ loading p_{py} : 1) 0.007, 2) 0.012, 3) 0.031, 4) 0.058, 5) 0.106, 6) 0.182. The Ox⁺ modification was one molecule at both ends of the channel, on average.

Table 3. Front-back trapping efficiencies $T_{\text{FB},\infty}$: a) as a function of different Py⁺ loadings p_{py} for crystals of about 0.65 μm (l_{cyl}), b) as a function of different crystal lengths l_{cyl} for a Py⁺ loading p_{py} of 0.11.

| a) | p_{py} | $T_{\text{FB},\infty}$ | b) | l_{cyl} [nm] | $T_{\text{FB},\infty}$ |
|----|-----------------|------------------------|----|--------------------------|------------------------|
| | 0.007 | 0.355 | | 300 | 0.905 |
| | 0.012 | 0.448 | | 500 | 0.773 |
| | 0.031 | 0.531 | | 850 | 0.512 |
| | 0.058 | 0.571 | | 1400 | 0.412 |
| | 0.106 | 0.673 | | 2400 | 0.329 |
| | 0.182 | 0.737 | | - | - |

excitation energy, initially located at the Py⁺, reaches the acceptor Ox⁺ and therefore the two ends of the crystal. Furthermore, we observe a shift of 15 nm to longer wavelengths in the Py⁺ emission, from 515 to 530 nm, with increasing loading, whereas the maximum of the Ox⁺ emission remains almost constant. This shift is probably due to self-absorption and reemission, as we have suggested^[7] and discussed more quantitatively before.^[8] A unified theory of radiative and radiationless energy transfer, which should also apply to this system, has recently been published.^[54]

3.3.2. Trapping Efficiency as a Function of the Crystal Length l_{cyl}

We expect that the trapping efficiency increases with decreasing crystal length l_{cyl} for otherwise constant parameters, specifically constant p_{py} , because the excitation energy has to migrate over an increasingly large distance to reach a trap. This can be tested if materials with different average crystal lengths are available over a significant range. Since we have been able to prepare this material, experiments with crystals of the following average length were carried out: 1) 300 nm, 2) 500 nm, 3) 850 nm, 4) 1400 nm, and 5) 2400 nm. These crystals were loaded with Py⁺ so that the occupation probability was always the same, namely $p_{\text{py}} = 0.11$. They were then modified with two Ox⁺ molecules on average at both ends of the channels. The fluorescence of a thin layer on quartz was measured at room

temperature after specific excitation of Py^+ at 460 nm. The fluorescence reported in Figure 11 is scaled to the same height at the Py^+ emission maximum, as before. We immediately recognize the very strong increase of the front-back trapping

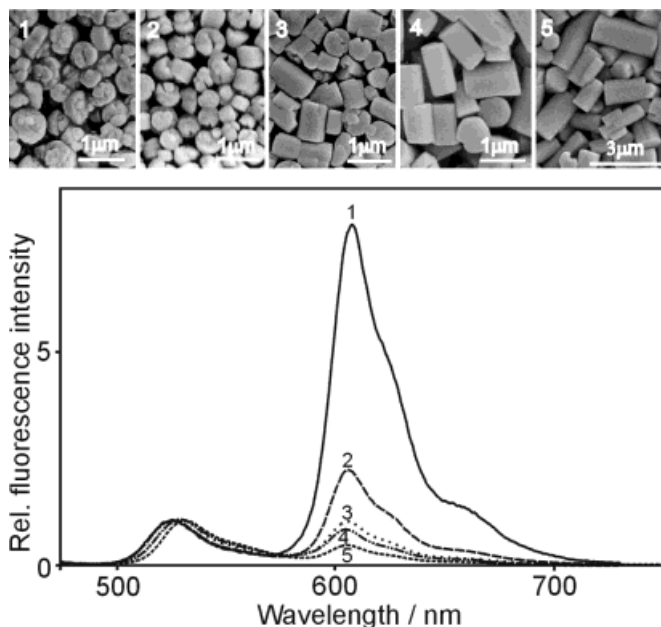


Fig. 11. Upper: EM pictures of the investigated zeolite L samples with different average crystal length l_{cyl} : 1) 300 nm, 2) 500 nm, 3) 850 nm, 4) 1400 nm, 5) 2400 nm. Lower: Fluorescence intensity after specific excitation of only Py^+ at 460 nm (scaled to the same height at the maximum of the Py^+ emission) of Py^+ loaded and Ox^+ modified zeolite L crystals with constant Py^+ loading ($p_{\text{py}} = 0.11$) as a function of crystal length. The Ox^+ modification was two molecules at both ends of the channel, on average.

efficiency from 0.33 up to 0.91 with decreasing crystal length l_{cyl} . This means that in the 300 nm crystals, 90 % of the emitted light is due to energy migration along the Py^+ and finally transferred to the luminescent traps Ox^+ . Interestingly, there is also in these experiments, carried out at constant Py^+ loading, a small shift of the Py^+ maximum, from 525 nm for the smallest crystals to 530 nm for the largest ones. The maximum of the Ox^+ emission remains at 605 nm. This wavelength shift is most probably due to self-absorption and re-emission because the absorption depth increases with increasing crystal size despite of the constant p_{py} .

3.3.3. Fluorescence Microscopy

The qualitative understanding of the material can be much improved by means of fluorescence microscopy pictures.^[6,9,15] Large crystals are especially illustrative for this purpose, that is why we show in Figure 12 two pictures of zeolite L crystals loaded with Py^+ and modified with Ox^+ from sample 5 (Fig. 11). Picture 1 shows some crystals after specific excitation of Py^+ at 470–490 nm. The separate regions which are occupied by the two dyes Py^+ and Ox^+ are clearly visible. We recall that the resolution of an optical microscope is in the order of half of the emitted wavelength. The middle region of the zeolite L

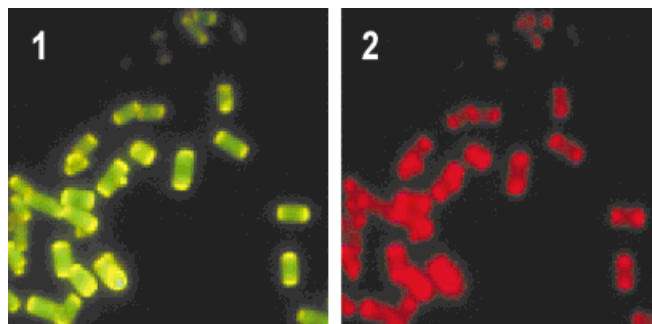


Fig. 12. True color microscope pictures of Py^+ loaded and Ox^+ modified zeolite L crystals of about 2400 nm (sample 5 of Fig. 11). Left: Fluorescence after excitation of Py^+ at 470–490 nm. Right: Fluorescence after excitation of Ox^+ at 545–580 nm.

crystal fluoresces green because of the Py^+ . The emission at both ends of the crystal appears yellowish due to mixing of the green Py^+ and the red Ox^+ emission. Ox^+ is not excited directly, but via energy transfer from Py^+ . The red Ox^+ emission seen in picture 2 is due to specific excitation of Ox^+ at 545–580 nm.

4. Discussion and Conclusions

The success of our investigations on inorganic–organic host–guest composites as optical antenna systems depends largely on the availability of a sufficiently broad size range of zeolite L crystals and of good methods to incorporate the guest molecules. This article concentrates on fine-tuning of the size of zeolite L crystals in the range of 30 nm to 3000 nm and on the preparation and characterization of crystals loaded with Py^+ as donor, modified with Ox^+ as acceptor. Control of the size and shape of zeolite L crystals is shown to be possible in a very versatile synthesis procedure by modifying the composition of the synthesis gel under otherwise similar reaction conditions. This allowed us to study the energy migration efficiency (trapping efficiency) of dye-loaded zeolite L crystals, as a function of the Py^+ loading and, specifically, as a function of crystal size in a large range.

4.1. Synthesis of Zeolite L

The basic procedure consists of mixing a strongly alkaline aluminum hydroxide solution with a colloidal aqueous silica suspension in a pressure tight Teflon reactor and crystallization of the product at 433 K. The composition of the synthesis gel is $(a\text{K}_2\text{O}-b\text{Al}_2\text{O}_3-c\text{SiO}_2-d\text{H}_2\text{O})$, where a , b , c , and d can be varied within a certain range, which we known from ternary crystallization diagrams.^[1] Small variations even within this range can have a big influence on size and morphology of the product. It is also important to control the quality of the starting materials. Differences can be observed when using SiO_2 suspensions from different companies. It is advisable to prepare the SiO_2 suspension in the laboratory freshly before use, in order to obtain reproducible results.

Increasing the H₂O content results in increasingly larger zeolite L crystals with smoother surface, because the viscosity of the synthesis gel decreases and therefore transport of the species in the gel becomes faster. Increasing the H₂O content by 25 % in a gel with the molar composition (2.55 K₂O–1 Al₂O₃–9.72 SiO₂–161.3 H₂O) yields crystals of about 3000 nm, see sample 5 in Figure 11. But a further increase of the amount of H₂O does not yield zeolite L.

Smaller crystals can be obtained by increasing the amount of K₂O. At the same time the tendency to form intergrowths at both ends of the cylinders increases. Zeolite L cylinders with a mono modal particle size distribution and a hydrodynamic radius of 295 nm crystallize from a synthesis gel with a K₂O/SiO₂ ratio of 0.339. The high alkalinity of such a gel can help in the uptake of material from the solid phase into solution and influence the crystallization time and the morphology of the material, as shown in Table 1 and Figure 5. It is, however, not clear which aspect is responsible for the suppression of the growth in *c*-direction and the enhanced inter growth tendency. Extremely alkaline conditions, but also a large SiO₂/Al₂O₃ ratio in the synthesis gel are needed to crystallize zeolite L in the range of 30 to 100 nm. Material of this type is obtained when using the gel composition (10 K₂O–1 Al₂O₃–20 SiO₂–400 H₂O).^[44,45]

We emphasize that a small variation of only one parameter in the zeolite synthesis may influence the crystallization process dramatically. It is therefore necessary to report a successful synthesis in sufficient detail, if the result should be reproducible.

4.2. Micropore Volume

Argon adsorption measurements at 87 K are a suitable tool to detect differences in the accessible pore volume of zeolite L. The commercial zeolite L shows a smaller specific surface area than the synthesized material despite of the smaller crystal size. The higher adsorption capacity of the self-synthesized material is due to a larger micropore volume. This follows from the higher adsorption in the region of micropore filling, see insert in Figure 9. Structural defects in the pore system of the commercial zeolite L are likely to be the cause. The shape of the Ar adsorption isotherms at small relative pressure (insert of Fig. 9) is meaningful.^[55] According to the literature^[32] it reflects the bimodal pore system of zeolite L that originates from the 8-ring and in the 12-ring channels, both accessible for Ar.

4.3. Bi-Directional Antenna Properties

Inorganic–organic host–guest composites as optical antenna systems were prepared by loading the crystals with Py⁺ as donor and modifying them at both ends of each channel with one or two acceptors Ox⁺, on average. The main difference of the results reported here with respect to our earlier investigations^[7] consists of the diversity and quality of zeolite L crystals that were available and in the more sophisticated way to prepare the dye loaded material. We took care that all aggregates on the zeolite surfaces were removed, in order to avoid lumi-

nescence quenching. The data reported in Figures 10 and 11 and also in Table 3 illustrate the large improvement of the new materials. The measurements were made on thin dye-loaded zeolite L layers on quartz plates, in contrast to those described in the literature^[7] which were carried out in an aqueous suspension. The pronounced increasing trapping efficiency with decreasing length of the zeolite L underlines the interpretation that the antenna behavior is mainly governed by Förster type energy transfer, supported by self-absorption and reemission. The latter cause a shift in the maximum of the Py⁺ fluorescence spectrum with increasing loading, but also with increasing crystal size at constant loading. Some internal reflection might also occur, especially in the larger crystals, where it increases the absorption probability. We conclude that all tools have now been prepared to penetrate deep into the photophysical processes of this fascinating bi-directional antenna system and to test its ability as luminescent microprobes for analytical purposes and for other applications as discussed in the literature.^[8,16]

5. Experimental

5.1. Materials

Synthesis of Zeolite L: The standard procedure of zeolite L synthesis is the preparation of a synthesis gel, e.g., with a molar composition of (2.99 K₂O–1 Al₂O₃–10.70 SiO₂–169.3 H₂O) from two separately prepared solutions (A and B). To obtain approximately 40 mL starting gel, solution A is prepared as follows: 1.475 g Al(OH)₃ (Fluka, purum) is dissolved under reflux in a solution consisting of 3.175 g KOH (>86 %, Fluka, Biochemika) and 6.225 g water until the mixture looks transparent. B) 20.253 g colloidal silica (AEROSIL K330, Degussa, 30 wt.-%) and 7.376 g doubly distilled water are mixed and kept in a ultrasonic bath for at least 10 min. After cooling to room temperature solution A is added to solution B while stirring strongly. During vigorous stirring this mixture turns into a thick opaque gel, which is then transferred into a cylindrical poly(tetrafluoroethylene) (PTFE) vessel (90 mm length, Ø 27 mm), which is placed in a tight PTFE pressure vessel (MLS GmbH, HPV80, 50 mL, 60 bar). Crystallization takes place without stirring at 433 K within 6 days. After crystallization the pressure vessel is cooled in icewater before opening. The upper part of the clear, strongly alkaline solution is decanted. The white residue is washed several times with hot doubly distilled water and centrifuged until the supernatant reacts neutral. The zeolite is then air dried for approximately 14 h at 100 °C. Approximately 5 g of zeolite L microcrystals with cylinder morphology of about 700 nm length and 600 nm diameter with a narrow size distribution are obtained. If it is not mentioned, the synthesis of zeolite L was performed under static conditions.

Variations: An important variation consists of changing the composition of the starting gel, e.g., the H₂O/SiO₂ and K₂O/SiO₂ ratios. We refer to Section 3 for details.

Dynamic crystallization means that the pressure vessels were rotating (–16 min^{–1}) at 433 K. For this, the reaction vessels were attached in a special holder in a drying oven which was mounted at an angle of approximately 30°. These conditions reduce the crystallization time to 2 days.

A further variation was the preparation of the colloidal silica suspension freshly before using it for the preparation of the silicate solution. The silica source (OX50, Degussa) was the same as that for the commercially available suspension (AEROSIL K330, Degussa). 15 g SiO₂ were added to 35 g doubly distilled water and suspended for 15 min at 22 000 min^{–1} (Turrax, IKA). This suspension was left for about 1 h and again treated for 5 min before using.

To obtain smaller zeolite L crystals, a gel with a molar composition of (10 K₂O–1 Al₂O₃–20 SiO₂–400 H₂O) was prepared. The synthesis was performed as reported [44] except the silica source and the reaction vessel were different. We used a freshly prepared suspension of colloidal silica as mentioned above. The starting solutions were pretreated for 15 h under reflux. Zeolite L crystals of about 30–100 nm size were obtained under dynamic crystallization conditions after 6 h at 443 K. These small zeolite L crystallites tend to form nanoclusters as described before [20,45].

Dyes: Pyronine (3,6-diamino-xanthylium, Py⁺) and oxonine (3,7-diaminophenoxazinyl, Ox⁺) were synthesized and purified according to the procedure in the literature [7].

Loading of Zeolite L with Py⁺/Ox⁺: The dye-loaded zeolite L crystals, used for the investigation of energy migration, were prepared as follows: 100 µL zeolite L aqueous suspension (1 g/50 mL) was added to 3 mL doubly distilled water containing the corresponding concentration of aqueous Py⁺ solution to reach the desired Py⁺ loading. This suspension was treated in an ultrasonic bath for at least 10 min in order to avoid aggregation of the microcrystals before refluxing for typically 4 h for the shorter crystals. The suspension was then centrifuged and the remaining dye concentration in the supernatant was analyzed. To modify the cylindrical microcrystals at each end with Ox⁺, the Py⁺ loaded sample was added to an aqueous Ox⁺ solution and refluxed for 30 min. The Ox⁺ loading is calculated so that on average one or two molecules, depending on the case, were placed at each end of the zeolite channels. For details we refer to ref. [7]. For the conditions applied Ox⁺ is incorporated quantitatively into the zeolite channels because of its large equilibrium constant.

NaClO/HCl-Treatment: The dyes can form aggregates at the outer zeolite surface. Aggregates at the surface and in solution can be eliminated with NaClO/HCl-solution, which is reflected in the enhancement of fluorescence intensity of the dye loaded sample. After the Ox⁺ modification equal volumes of 2 × 10⁻³ M NaClO (Dr. Grogg Chemie AG Bern, techn.) and 2 × 10⁻³ M HCl (Merck, p.a.) are added stepwise one after another to the dye loaded sample and the fluorescence is measured. The dye aggregates are assumed to be eliminated, when the fluorescence remains constant.

HF-Treatment: To determine the dye loading, the zeolite L framework is decomposed in HF solution. 300 µL HF (40%, Merck, p.a.) are given to approximately 2 mg of the dye loaded zeolite L sample to destroy the zeolite framework. Afterwards 700 µL 4 M NaOH solution and 1 mL doubly distilled water are added for neutralization. The precipitate is centrifuged. For the determination of the dye concentration in the zeolite an ultraviolet-visible (UV-vis) spectrum of the supernatant is measured. From this, the loading could be calculated. Tests have shown that the dyes are not affected by this procedure.

Preparation of Thin Films: After the treatment with NaClO/HCl 250 µL (approximately 1.3 mg/mL) of the aqueous dye-loaded zeolite L suspension is dropped on a quartz plate with a diameter of 1.6 cm. The quartz plate is cleaned with ethanol and doubly distilled water. The suspension is allowed to dry in air overnight covered with a Petri dish.

5.2. Physical Measurements

The materials were characterized by X-ray powder diffraction with a “Guinier-camera de Wolff Mk.IV” from ENRAF-NONIUS and an STOE powder diffractometer STADI P. Thermogravimetric measurements were performed with Thermowaage TG 50 from Mettler. EM-pictures were recorded with a JOEL JSM 840 raster electron microscope. Energy dispersive X-ray (EDX) measurements were carried out with a NORAN TN 5402 spectrometer. TEM images were measured on a Hitachi H-600-2 electron microscope at 100 kV acceleration voltage. DLS measurements were performed with an ALV-NIBS high-performance particle sizer from ALV (ALV-Laser GmbH, Langen, DE). Ar adsorption isotherms were measured with a Sorptomatic 1990 including krypton unit from CE-Instruments using argon as adsorbate at ~87 K in the range of partial pressure 10⁻⁴ to 1. Approximately 0.3 to 0.4 mg of the zeolite was thermally activated up to 623 K with a rate of 0.5 K/min in high vacuum (HV). The samples were kept at least 15 h under these conditions until the residual pressure was <10⁻⁴ torr. In the low-pressure region ($p/p_0 < 0.015$) equilibrium was assumed when the pressure over the sample did not change by more than 0.005 torr within 7 min. To evaluate the data we used the software package of Sorptomatic 1990 as well as Milestone 2000 Physisorption Software Advanced Data Processing 4.0. We calculated the specific surface area with the Langmuir ($p/p_0^0: 0.05-0.25$) method as well as the BET ($p/p_0^0: 0.01-0.20$) method. We determined the micropore volume with help of the method of Saito/Foley (Ar on zeolite at 87.3 K) and at the relative pressure p/p_0 of 0.95. UV-vis spectra were recorded on a Lambda 14 spectrophotometer (Perkin Elmer). Fluorescence spectra were measured with a luminescence spectrometer LS 50B (Perkin Elmer) in suspensions at 1 cm quartz cuvettes and on thin layers. Optical microscopy pictures of fluorescent samples were taken with 1000 times enlargement on an Olympus BX 60 microscope combined with a Kappa CF 20 DCX Air K2 charge coupled device (CCD) camera. The light stemming from a 100 W halogen or mercury lamp was passed through appropriate excitation cubes comprised of a narrow band excitation filter, a dichroic mirror and a cut-off barrier filter. For the observation of the Py⁺ and Ox⁺ fluorescence the appropriate cubes were selected to excite the investigated molecules in the region of the first π,π^* absorption band: (470–490 nm) and (545–580 nm). Images were recorded with KappaImageBase software.

Received: December 27, 2000
Final version: May 29, 2001

- [1] D. W. Breck, *Zeolite Molecular Sieves*, Wiley, New York 1974.
- [2] W. M. Meier, D. H. Olson, C. Bärlocher, *Atlas of Zeolite Structure Types*, Elsevier, London 1996.
- [3] T. Ohsuna, Y. Horikawa, K. Hiraga, *Chem. Mater.* 1998, 10, 688.
- [4] F. Binder, G. Calzaferri, N. Gfeller, *Sol. Energy Mater. Sol. Cells* 1995, 38, 175.
- [5] N. Gfeller, G. Calzaferri, *J. Phys. Chem.* 1997, 101, 1396.
- [6] N. Gfeller, S. Megelski, G. Calzaferri, *J. Phys. Chem. B* 1998, 102, 2433.
- [7] N. Gfeller, S. Megelski, G. Calzaferri, *J. Phys. Chem. B* 1999, 103, 1250.
- [8] G. Calzaferri, D. Brühwiler, S. Megelski, M. Pfenniger, M. Pauchard, B. Hennessy, H. Maas, A. Devaux, U. Graf, *Solid State Sci.* 2000, 2, 421.
- [9] M. Pfenniger, G. Calzaferri, *Chem. Phys. Chem.* 2000, 4, 211.
- [10] U. Vietze, O. Krauss, F. Laeri, G. Ihlein, F. Schüth, B. Limburg, M. Abraham, *Phys. Rev. Lett.* 1998, 81, 4628.
- [11] V. Ramamurthy, in *Photochemistry in Organized and Constraint Media* (Ed: V. Ramamurthy), John Wiley & Sons, New York 1991, Ch. 10.
- [12] L. Werner, J. Caro, G. Finger, J. Kornatowski, *Zeolites* 1992, 12, 658.
- [13] T. Bein, *Chem. Mater.* 1996, 8, 1636.
- [14] F. Schüth, *Chem. Unserer Zeit* 1995, 29, 45.
- [15] S. Megelski, A. Lieb, M. Pauchard, A. Drechsler, S. Glaus, C. Debus, A. Meixner, G. Calzaferri, *J. Phys. Chem.* 2001, 105, 25.
- [16] G. Calzaferri, *Chimia* 1999, 52, 525.
- [17] W. T. Koetsier, J. P. Verduijn, *Eur. Patent 185 519*, 1986.
- [18] M. T. Wortel, J. P. Verduijn, *Eur. Patent 220 881*, 1987.
- [19] S. Ernst, J. Weitkamp, *J. Catal. Today* 1994, 19, 27.
- [20] M. Lovallo, M. Tsapatsis, *Adv. Catal. Nanostruct. Mater.* 1996, 307.
- [21] J. M. Newsam, *J. Phys. Chem.* 1989, 93, 7689.
- [22] R. M. Barrer, H. Villiger, *Z. Kristallogr.* 1969, 128, 352.
- [23] M. Sato, K. Morikawa, S. Kurosawa, *Eur. J. Mineral.* 1990, 2, 851.
- [24] E. F. Vansan, G. Peeters, *J. Chem. Soc., Faraday Trans. 1* 1977, 73, 1574.
- [25] P. A. Newell, L. V. C. Rees, *Zeolites* 1983, 3, 28.
- [26] A. Burton, R. F. Lobo, *Microporous Mesoporous Mater.* 1999, 33, 97.
- [27] B. Hennessy, S. Megelski, C. Marcolli, V. Shklover, C. Bärlocher, G. Calzaferri, *J. Phys. Chem. B* 1999, 103, 3340.
- [28] L. Barbosa, G. Calzaferri, *Res. Chem. Intermed.* 1995, 21, 25.
- [29] D. W. Breck, E. M. Flanigen, *Molecular Sieves*, Society of Chemical Industry, London 1968, p. 47.
- [30] M. Pauchard, A. Devaux, G. Calzaferri, *Chem. Eur. J.* 2000, 6, 3456.
- [31] R. Seifert, R. Rytz, G. Calzaferri, *J. Phys. Chem. A* 2000, 104, 7473.
- [32] P. E. Hathaway, M. E. Davis, *Catal. Lett.* 1990, 5, 333.
- [33] K. S. W. Sing, D. H. Everett, R. A. W. Haul, L. Moscou, R. A. Pierotti, J. Rouquerol, T. Siemieniowska, *Pure Appl. Chem.* 1985, 57, 603.
- [34] K. S. W. Sing, *Thesis, Reporting Physisorption Data for Gas/Solid Systems, IUPAC* 1982, 54, 11, 2201.
- [35] K. S. W. Sing, *J. Porous Mater.* 1995, 2, 5.
- [36] Deutsche Norm, DIN 66 131, July 1993.
- [37] a) S. J. Gregg, K. S. W. Sing, *Adsorption, Surface Area and Porosity*, Academic, London 1982. b) F. Rouquerol, J. Rouquerol, K. Sing, *Adsorption by Powders & Porous Solids*, Academic, London 1999.
- [38] A. Saito, H. C. Foley, *AIChE J.* 1991, 37, 429.
- [39] R. Zostak, *Molecular Sieves*, Blackie Academic & Professional, Thomson Science, London 1998, Ch. 4.
- [40] D. W. Breck, N. A. Acara, Union Carbide Corporation, *US Patent 909 264*, 1962.
- [41] D. E. W. Vaughan, *Eur. Patent 142 349*, 1985.
- [42] J. P. Verduijn, *Eur. Patent 219 354*, 1987.
- [43] P. V. Verduijn, J. Mechilium, C. B. De Gruyter, W. T. Koetsier, C. W. M. Van Oerschoot, *US Patent 5 064 630*, 1991.
- [44] X. Meng, Y. Zhang, C. Meng, W. Pang, in *Proc. 9th Int. Zeolite Conf.*, Montreal 1992 (Eds: R. Ballmoos, J. B. Higgins, M. M. J. Treacy), Butterworth-Heinemann 1993.
- [45] a) M. Tsapatsis, T. Okubo, M. Lovallo, M. E. Davis, *Mater. Res. Soc. Symp. Proc.* 1995, 371, 21. b) M. Tsapatsis, M. Lovallo, T. Okubo, M. E. Davis, M. Sadakata, *Chem. Mater.* 1995, 7, 1734.
- [46] Y. S. Ko, W. S. Ahn, *Bull. Korean Chem. Soc.* 1999, 20, 173.
- [47] Y. S. Ko, W. S. Ahn, J. H. Chae, S. H. Moon, *Stud. Surf. Sci. Catal.* 1997, 105, 733.
- [48] G. A. Ozin, A. Kuperman, A. Stein, *Angew. Chem.* 1989, 101, 373.
- [49] G. D. Stucky, J. E. Mac Dougall, *Science* 1990, 247, 669.
- [50] G. Calzaferri, N. Gfeller, *J. Phys. Chem.* 1992, 96, 3428.
- [51] V. Ramamurthy, D. R. Sanderson, D. F. Eaton, *J. Am. Chem. Soc.* 1993, 115, 10438.
- [52] D. Brühwiler, N. Gfeller, G. Calzaferri, *J. Phys. Chem. B* 1998, 102, 2923.
- [53] T. Förster, *Fluoreszenz organischer Verbindungen*, Vandenhoeck & Ruprecht, Göttingen 1951.
- [54] G. Juzeliūnas, D. L. Andrews, in *Resonance Energy Transfer* (Eds: D. L. Andrews, A. A. Demidov), Wiley, Chichester, UK 1999, p. 65.
- [55] S. Megelski, *Ph.D. Thesis*, University of Berne, Switzerland 2000.